Physics of the Earth and Planetary Interiors 196-197 (2012) 62–74

Contents lists available at SciVerse ScienceDirect

Physics of the Earth and Planetary Interiors

journal homepage: www.elsevier.com/locate/pepi

Slab-induced waveform effects as revealed by the TAIGER seismic array: Evidence of slab beneath central Taiwan

Po-Fei Chen [a,*], Craig R. Bina [b], Hao Kuo-Chen [c], Francis T. Wu [c], Chien-Ying Wang [a], Bor-Shouh Huang [d], Chau-Huei Chen [e], Wen-Tzong Liang [d]

[a] Department of Earth Sciences and Institute of Geophysics, National Central University, Taoyuan, Taiwan
[b] Department of Earth and Planetary Sciences, Northwestern University, Evanston, IL, United States
[c] Geological Sciences, State University of New York at Binghamton, Binghamton, NY, United States
[d] Institute of Earth Sciences, Academia Sinica, Taipei, Taiwan
[e] Department of Earth and Environment Science, National Chung Cheng University, Chiayi, Taiwan

ARTICLE INFO

Article history:
Received 3 October 2011
Received in revised form 11 January 2012
Accepted 6 February 2012
Available online 15 February 2012

Keywords:
TAIGER
Broadband linear array
Slab-induced waveform effects
Pseudospectral method

ABSTRACT

Here we tackle a tectonically important question – the upper mantle velocity structure beneath central Taiwan – with seismically interesting observations – receiver-side slab waveform effects. We use teleseismic P waveforms of the NS broadband array deployed by the TAIGER project to examine patterns of variation in arrival time, pulse width, and amplitude – measuring the first two by Gaussian fitting – and contrast measurements of earthquakes to the southeast (SE earthquakes) with those of one Sumatra earthquake in order to focus on upper mantle heterogeneities. Overall variation patterns as a function of earthquake are compatible with ray-tracing predictions. Relative reduced arrival times and amplitudes at central Taiwan stations suggest the existence of a deep aseismic slab below. From simulations of 2-D wave propagation, we conclude that lateral heterogeneity of crust and uppermost mantle primarily contributes to variations in arrival time and only secondarily to variations in amplitude and pulse width. Furthermore, discrepancies between source-side and receiver-side waveform effects, where the latter are not always amplitude-reduced, are explained by constructive interference between the fast and slow phase. Thus, the use of full waveform information can provide independent constraints to complement results of previous studies. A future extension will be to incorporate S waves and apply waveform inversion to yield quantitative constraints.

1. Introduction

In the vicinity of Taiwan, the 8 cm/yr or so convergence rates of the Eurasia Plate (EUP) and the Philippine Sea Plate (PSP) are mainly accommodated by two subduction systems with opposing polarity: the east-dipping EUP slab and the predominantly northwest-dipping PSP slab, respectively to the south and northeast of Taiwan. It is widely accepted that the mountains we see today in Taiwan are a result of collisions between the southeast Asian continent and the Luzon arc, initiated a few Ma ago and continuing to date (Ho, 1986; Teng, 1990; Malavieille et al., 2002). What remains a matter of debate, however, is whether these collisions involve the entire EUP lithosphere (thick-skinned model; Wu et al., 1997) or only the crustal portion (thin-skinned model; Suppe, 1981). In the thick-skinned model, the lithospheres of the Philippine Sea plate and the Eurasian plate are engaged in collision without subduction of either plate (Wu et al., 1997), thus favoring the absence of slab in the upper mantle beneath central Taiwan. On the other hand, in the thin-skinned model, orogeny is essentially caused by the deformation of the accretionary wedge above a passively subducting lithosphere (Davis et al., 1983), thus favoring the presence of an aseismic slab. However, termination of the Manila trench offshore of southwest Taiwan and of the Wadati-Benioff zone beneath southern Taiwan have obscured resolution of this puzzle, one that is critical to understanding the tectonic evolution and orogenic processes of Taiwan.

This question generally has been approached along two lines, characterized by starkly different philosophies. On the one hand, ever since the first tomographic images of upper mantle structure beneath Taiwan (Bijwaard et al., 1998) became available, resolution has been progressively enhanced by collecting more global datasets (Lallemand et al., 2001; Li and van der Hilst, 2010) and by incorporating arrival times of local earthquakes into a joint inversion (Wang et al., 2009). Efforts along this line culminate in the recent Taiwan Integrated Geodynamic Research (TAIGER) pro-

* Corresponding author. Address: Institute of Geophysics, National Central University, No. 300, Jhongda Rd, Jhongli City, Taoyuan 320, Taiwan, ROC. Tel.: +886 3 4227151 65647.
E-mail address: bob@ncu.edu.tw (P.-F. Chen).

0031-9201/$ - see front matter © 2012 Elsevier B.V. All rights reserved.
doi:10.1016/j.pepi.2012.02.004

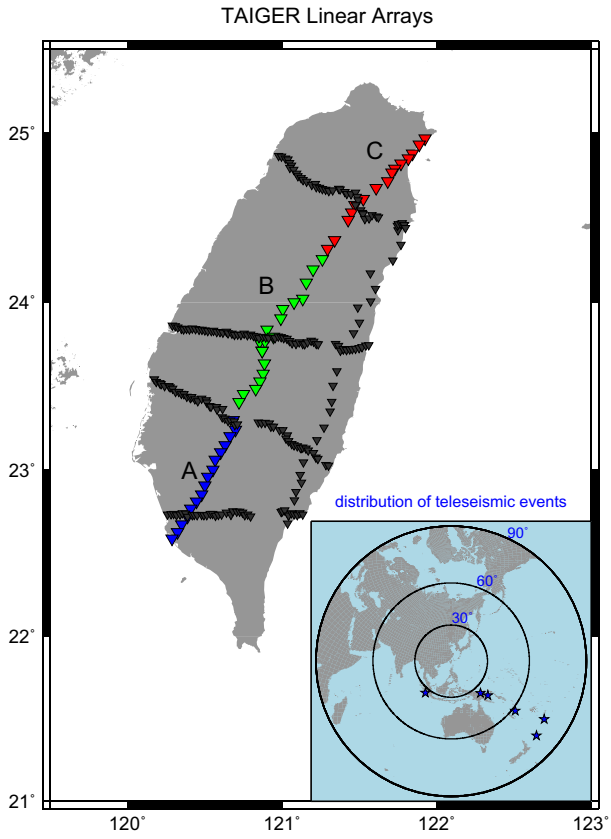

Fig. 1. Distribution of six dense linear arrays deployed during the TAIGER project, with stations of NS array colored blue (group A), green (group B), and red (group C). Inset shows distribution of teleseismic earthquakes used in this study.

ject (Okaya et al., 2009), in which data from passive and active sources as observed by broadband and short-period seismic networks, short-period sensors (Texans), and ocean bottom seismometers are incorporated (Kuo-Chen, 2011). On the other hand, in what we refer as the "delicate" approach, limited numbers of data are carefully selected, and special geometrical relationships are employed, so as to directly observe seismic signatures of upper mantle structure beneath central Taiwan (Chen et al., 2004; Lin, 2009; Chen et al., 2011). Although not specifically envisioned by TAIGER, the dense linear seismic arrays deployed by the project (Fig. 1) indeed open up opportunities for studies using the delicate approach, which set the tone of this study. Here, we not only use information from full waveforms, but we also eliminate crustal effects by differentiating observations of earthquakes from one side of the array relative to the other, in order to extract seismic imprints of upper mantle structures.

Having recognized that Taiwan is a natural laboratory for observing waveform effects of slab material at the receiver side, due to its unique tectonic setting, the six linear seismic arrays deployed by project TAIGER between February 2009 and June 2009 (Fig. 1) are suitable for detecting spatial variations in seismic waveforms, given the dense nature (~6 km interval) of the arrays covering a broad aperture (~200 km). We conduct such experiments using data from teleseismic earthquakes, at such epicentral distances that the spatial variations of waveforms are attributable to lateral heterogeneity in the crust and upper mantle at the receiver side. The waveform information is described by arrival time, pulse width, and amplitude, with the first two being measured by Gaussian fitting. Values of the three parameters obtained from first P arrivals of SE earthquakes, as recorded by the broadband NS array, are subtracted from those of one Sumatra earthquake from the west. The resulting patterns as a function of epicentral distance (or incident angle) are examined in the framework of the relative lengths of rays within slab material, which is determined by combining results from 1-D ray tracing and known slab geometries. As subducting slab material is the most prominent feature known in the upper mantle beneath Taiwan, observations thus extracted should largely exhibit effects of such material, which have been detected numerically as early arrivals, reduced amplitudes, and broadened pulse widths (Vidale, 1987). We expect the approach adopted in this study will complement results of tomographic studies in the future, when waveform information is effectively measured (e.g., Sigloch and Nolet, 2006) for inversion, as waveforms are more sensitive to velocity contrasts than are arrival times.

While waveform effects of slab material constitute the main tool used here to address questions beneath Taiwan, the tool itself is interesting seismically. Whereas most observations focus on the source side (e.g., Silver and Chan, 1986; Lay and Young, 1989), a focus on the receiver side involves the more stringent requirement of a seismic array deployed in a subduction setting. Song and Helmberger (2007) used waveform and amplitude components as observed by the LA RISTRA transect in the southwestern United States to validate and establish structural geometry, sharpness, and velocity contrast as derived by previous regional tomographic studies. We expect that the waveforms recorded by TAIGER arrays will exhibit more distortion due to receiver-side slab for the relatively shallow, active Wadati-Benioff zone in the vicinity of Taiwan, thereby providing greater insight into waveform effects of receiver-side slab. To numerically distinguish between effects at the source side and the receiver side and to explain the observed pulse complexity at some stations, we simulate 2-D wave propagation by a pseudospectral method (Huang, 1992), investigating waveform effects at both sides as well as cases of crustal heterogeneity. Following the same data-analysis procedures as applied to actual observations, we conclude that crustal heterogeneities mostly contribute to the arrival times and only to a lesser extent to the amplitudes and pulse widths. While the source-side slab always induces early arrivals, reduced amplitudes, and broadened pulse widths, this is not always the case at the receiver side. Indeed, at some locations the amplitudes are actually enhanced and coupled with pulse-width reduction, which is explained by interference between the fast phase in the slab and the slow phase in ambient mantle.

Table 1
Parameters of teleseismic events from the Global CMT catalogue.

Event (#)	Date	Origin time	Long. (°)	Lat. (°)	Depth (km)	M_0 (dyn-cm)	*Mw*
1	19/3/2009	18:17:40.9	−174.660	−23.050	34	3.4e + 27	7.6
2	1/4/2009	3:54:58.8	144.100	−3.520	10	5.1e + 25	6.4
3	15/4/2009	20:01:34.4	100.470	−3.120	20	3.2e + 25	6.3
4	12/5/2009	1:26:26.1	149.540	−5.650	84	1.7e + 25	6.1
5	16/5/2009	0:53:52.7	−178.790	−31.520	55	7.2e + 25	6.5
6	2/6/2009	2:17: 3.5	167.950	−17.760	15	4.2e + 25	6.4

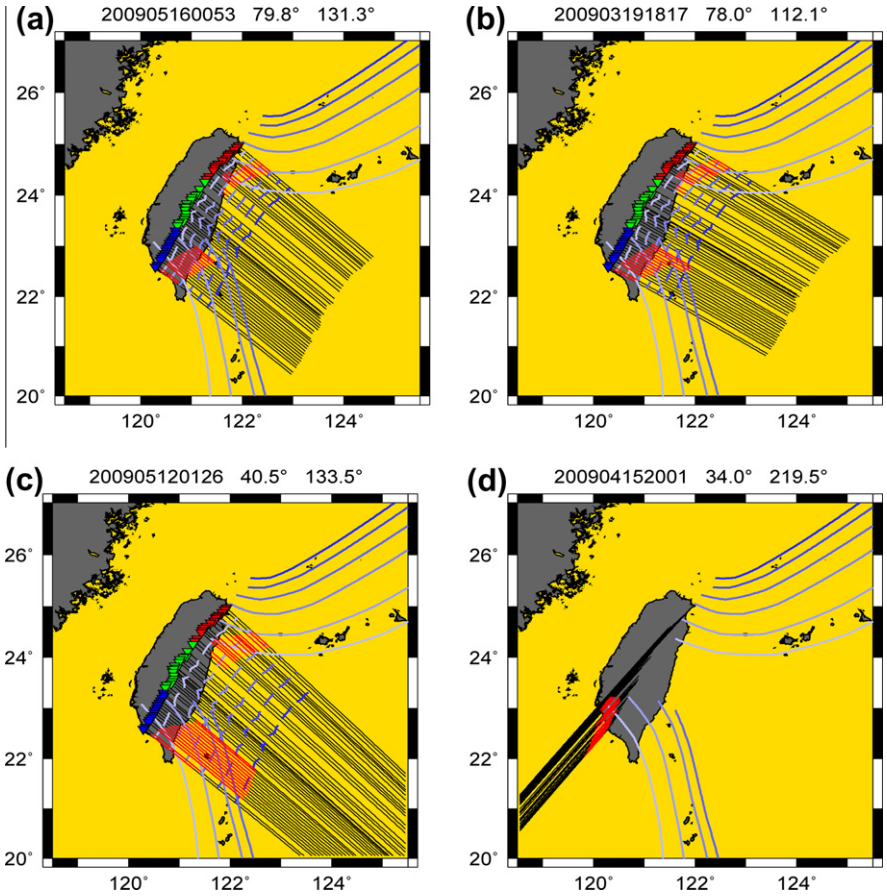

Fig. 2. Approaching rays (black lines), projected onto the surface, for four example earthquakes, with wavefront isodepths shown as dashed lines at 50-km intervals from 50 km (light blue) to 300 km (dark blue). Contours of a conceptual slab surface for the Manila and Ryukyu slabs are also displayed, as solid lines with the same color key. Ray segments within slab are colored red. Stations (triangles) of the three groups are color-coded as in Fig. 1. Event date, epicentral distance, and back azimuth, respectively, are shown at the top of each panel.

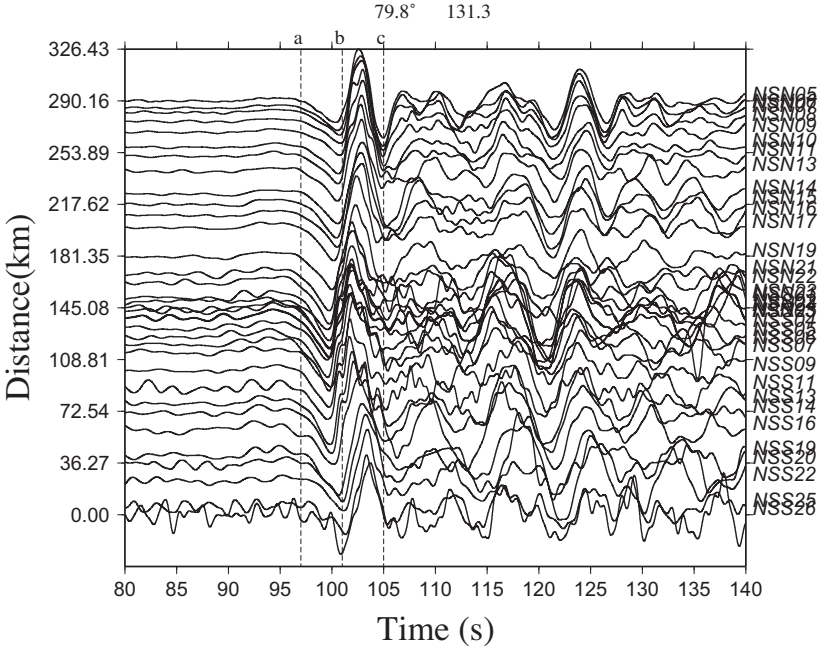

Fig. 3. Time-distance plot showing waveforms of teleseismic P from one of the SE earthquakes. Epicentral distance and back azimuth, respectively, are shown at top. Station codes appear to the right. Interval *bc* is window of extraction for Gaussian fitting, while *ac* is used for amplitude measurement. Note the significant variation of P waveforms across the array.

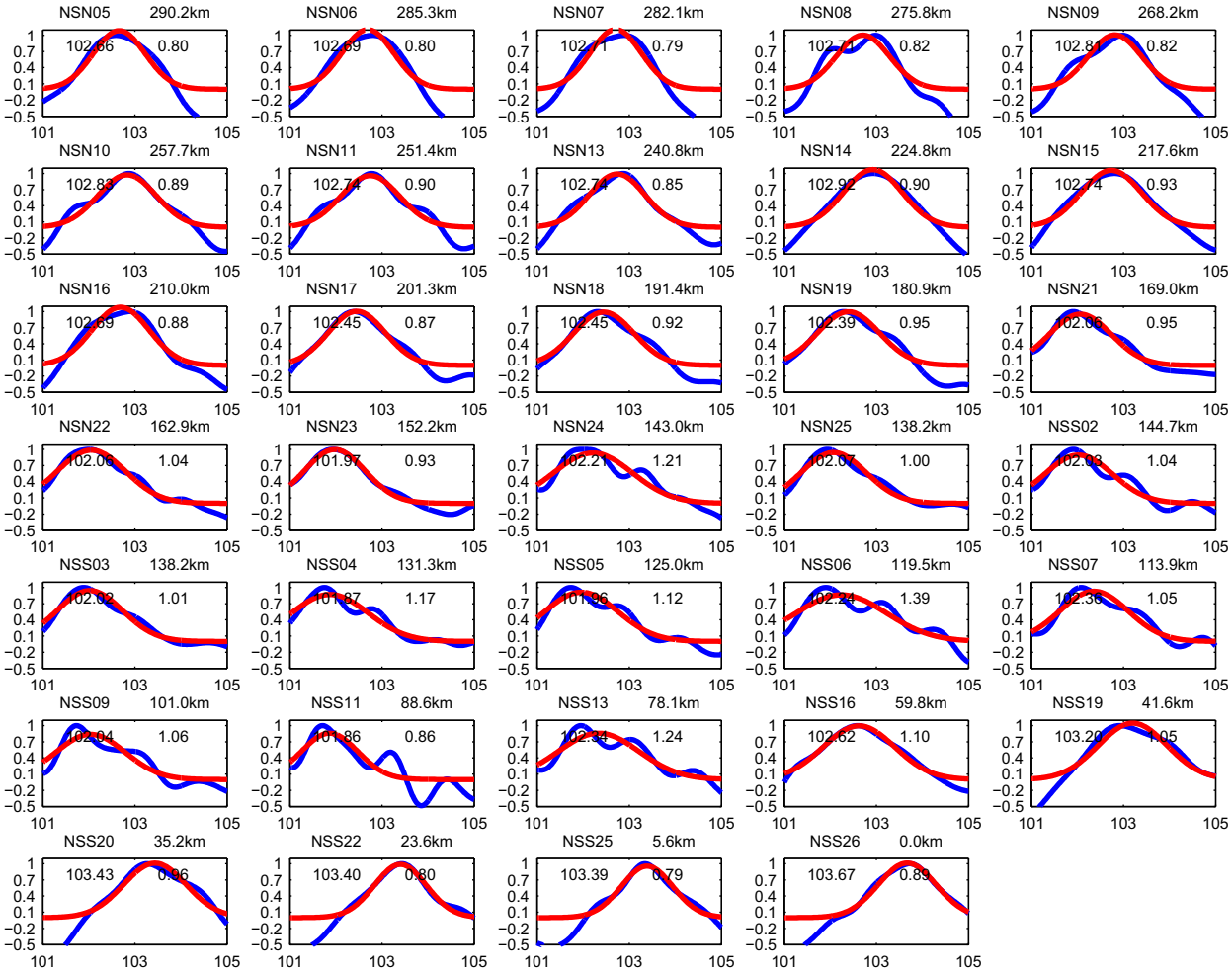

Fig. 4. Results of Gaussian fitting for normalized primary P waveforms, in order from north to south, shown as normalized amplitude *vs.* time in s. Blue curves are observations, and red curves are best-fit Gaussians, where numbers in box give mean and variance, respectively. Station names and distances, relative to the southernmost station, are shown above each box. Note the pulse complexity of waveforms for stations between 70 and 140 km. (For interpretation of the references to colour in this figure legend, the reader is referred to the web version of this article.)

2. Data and methods

2.1. Determine lengths of rays within slab

We extract earthquakes during the period of the TAIGER array deployment from the Global CMT catalogue (Ekström et al., 2005). Five significantly sized teleseismic earthquakes from the southeast (SE earthquakes) with epicentral distances ranging from 35° to 80° are selected (Fig. 1). The back azimuths of those SE earthquakes are nearly perpendicular to the azimuth of the NS array, suitable for investigating variation patterns as a function of incident angle. We also include observations of an earthquake from the west (Sumatra) for contrast. Table 1 shows earthquake parameters. We apply a fast marching method (Rawlinson et al., 2006) for 1-D ray tracing to stations of the NS array, and only those in the crust and upper mantle beneath the receiver side are considered. Isodepth contours of ray paths and of the slab surface (Simon Richards, pers. comm., 2010, http://www.4dearth.net) are drawn with the same color key (Fig. 2). For ray paths of SE earthquakes, we group the NS array into three groups – A, B, and C – from south to north, corresponding to the effects of the east-dipping Eurasian slab, the lateral heterogeneity of upper mantle beneath central Taiwan, and the north-dipping Philippine Sea slab, respectively (Figs. 1 and 2). Assuming the thickness of subducting slab is about 100 km in general, we mark with red those rays whose depths are below the slab surface at the same location and whose differences are no more than 100 km. As a result, the lengths of rays in red indicate the lengths of rays within slab material for specific source-receiver pairs (Fig. 2).

2.2. Determine relative arrival times, amplitudes, and pulse widths

Having deconvolved vertical component seismograms with instrument response, integrated to displacements, and filtered with 0.1–1.2 Hz bandpass, we plot waveforms of teleseismic events as recorded by the NS array using distances relative to the southernmost station as *y*-axis, while the *x*-axis is the time calibrated with 1-D theoretical arrival times (Kennett et al., 1995) and reset P arrivals at 100 s (Fig. 3). A time window is then assigned by visual inspection to extract only the half sinusoidal curves of the primary P waveform for Gaussian fitting (Fig. 4). The optimal means and standard deviations of waveforms thus fitted by Gaussians are taken as the arrival times and pulse widths, respectively (Fig. 4). We note that stations with distances ranging from 70 to 140 km tend to exhibit pulse complexities of bimodal distributions for SE earthquakes (Fig. 4), whose origin will be discussed later. The amplitudes are the peak-to-trough measurements using broader windows to include the full cycle of primary P (*ac* in

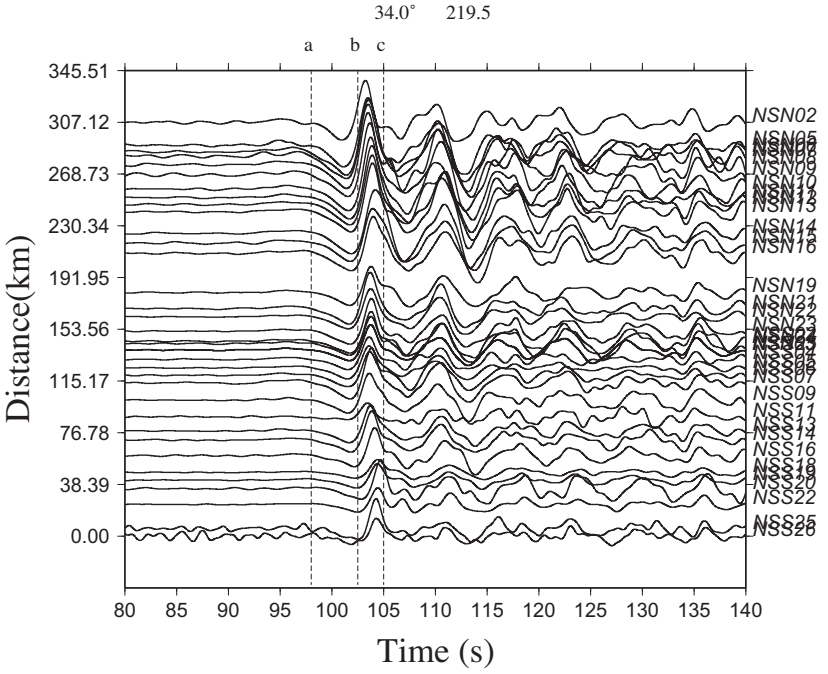

Fig. 5. Similar to Fig. 3, but for the Sumatra earthquake to the west. Note the high degree of waveform similarity among stations.

Fig. 3). By contrast, identically processed data from the Sumatra earthquake to the west exhibit a higher degree of waveform similarity among stations of the NS array (Fig. 5), suggesting that upper mantle structures to the east are more heterogeneous than those to the west of Taiwan. We use observations of the Sumatra earthquake as a reference. The differential relative arrival time (dif_art), pulse width (dif_wid), and amplitude (dif_amp) are thus determined as follows:

$$\mathrm{dif\_art}_i^{\mathrm{SE}} = (\mathrm{art}_i^{\mathrm{SE}} - \mathrm{art}_{\mathrm{mean}}^{\mathrm{SE}}) - (\mathrm{art}_i^{W} - \mathrm{art}_{\mathrm{mean}}^{W}) \quad (1)$$

$$\mathrm{dif\_wid}_i^{\mathrm{SE}} = (\mathrm{wid}_i^{\mathrm{SE}}/\mathrm{wid}_{\mathrm{mean}}^{\mathrm{SE}}) - (\mathrm{wid}_i^{W}/\mathrm{wid}_{\mathrm{mean}}^{W}) \quad (2)$$

$$\mathrm{dif\_amp}_i^{\mathrm{SE}} = (\mathrm{amp}_i^{\mathrm{SE}}/\mathrm{amp}_{\mathrm{mean}}^{\mathrm{SE}}) - (\mathrm{amp}_i^{W}/\mathrm{amp}_{\mathrm{mean}}^{W}) \quad (3)$$

where the subscript i indicates a particular station, the superscript SE a particular SE earthquake, the superscript W the reference Sumatran earthquake, and the subscript mean the average value for the event. For each SE earthquake, the mean of dif_art is calculated, and the value at each station relative to the mean is derived and then normalized for the earthquake. The same procedure is performed for dif_wid and dif_amp. Finally, we plot the normalized deviation of dif_art, dif_wid, and dif_amp for each earthquake using red circles, blue squares, and green triangles, respectively (Fig. 6).

2.3. Simulating waveform effects of crust, source-side slab, and receiver-side slab

We apply a pseudospectral method (Huang, 1992) to simulate two-dimensional wave propagation. The periods of waveforms are around 5 s, and the antiplane problem is invoked for simplicity. A virtual array is set up to record the propagating waves. Four scenarios are designed for the following purposes (Fig. 7): (1) to reproduce the effects of source-side slab similar to those of Vidale (1987); (2) to assess the effects of crust and uppermost mantle; (3) to assess the effects of warm slab on the receiver side; (4) to assess the effects of cold slab on receiver side. Accordingly, scenario 1 is built using a point source inside a 10% fast anomaly (Fig. 7a); scenario 2 uses a velocity profile beneath the NS array down to 200 km depth taken from an existing tomographic model (Fig. 7b; Wu et al., 2007); scenario 3 simulates an upward-propagating plane wave approaching a 3% fast anomaly (Fig. 7c); scenario 4 increases the fast anomaly of scenario 3–6% and moves it upward to touch the surface in order to eliminate effects of wavefront healing (Fig. 7d; Hung et al., 2001). We construct the virtual array with a distribution resembling the TAIGER NS array.

3. Results and interpretations

3.1. Various lengths of rays within slab as a function of earthquake

For rays to group A stations, we consider EUP slab only, and for rays to group C stations, we consider PSP slab only. All rays to group B stations are free of slab interactions for the moment, as limited by the empty slab contours, which will be tested later by observations. Fig. 2 demonstrates that, given the tectonic setting, it is inevitable that ray paths of teleseismic events to Taiwan will experience slab effects at the receiver side. To what extent these effects are exhibited depends upon where the earthquakes are located. For SE earthquakes, the results suggest that group A stations will exhibit more slab effects for earthquakes with epicentral distances ~40° (Fig. 2c) than for ~80° earthquakes (Fig. 2a and b), whereas the differences for group C stations are less obvious (Fig 2a, b, and c). This can be explained by the relationship between directions of approaching rays and of slab dip – nearly 0° for group A and nearly 180° for group B. For the Sumatran earthquake from the west, the slab effects are deemed to be minor (Fig. 2d).

3.2. Patterns of differential arrival times (dif_art), differential pulse width (dif_wid), and differential amplitudes (dif_amp)

Almost all five SE earthquakes exhibit a clear positive correlation between dif_art and dif_amp and a clear negative correlation between dif_art and dif_wid (Fig. 5). As will be demonstrated later by simulation results, this correlation and anti-correlation suggest that slab effects are dominant in the observations. Furthermore, among events, reductions of dif_art and dif_amp for group A stations relative to other groups are greatest for ~40° earthquakes,

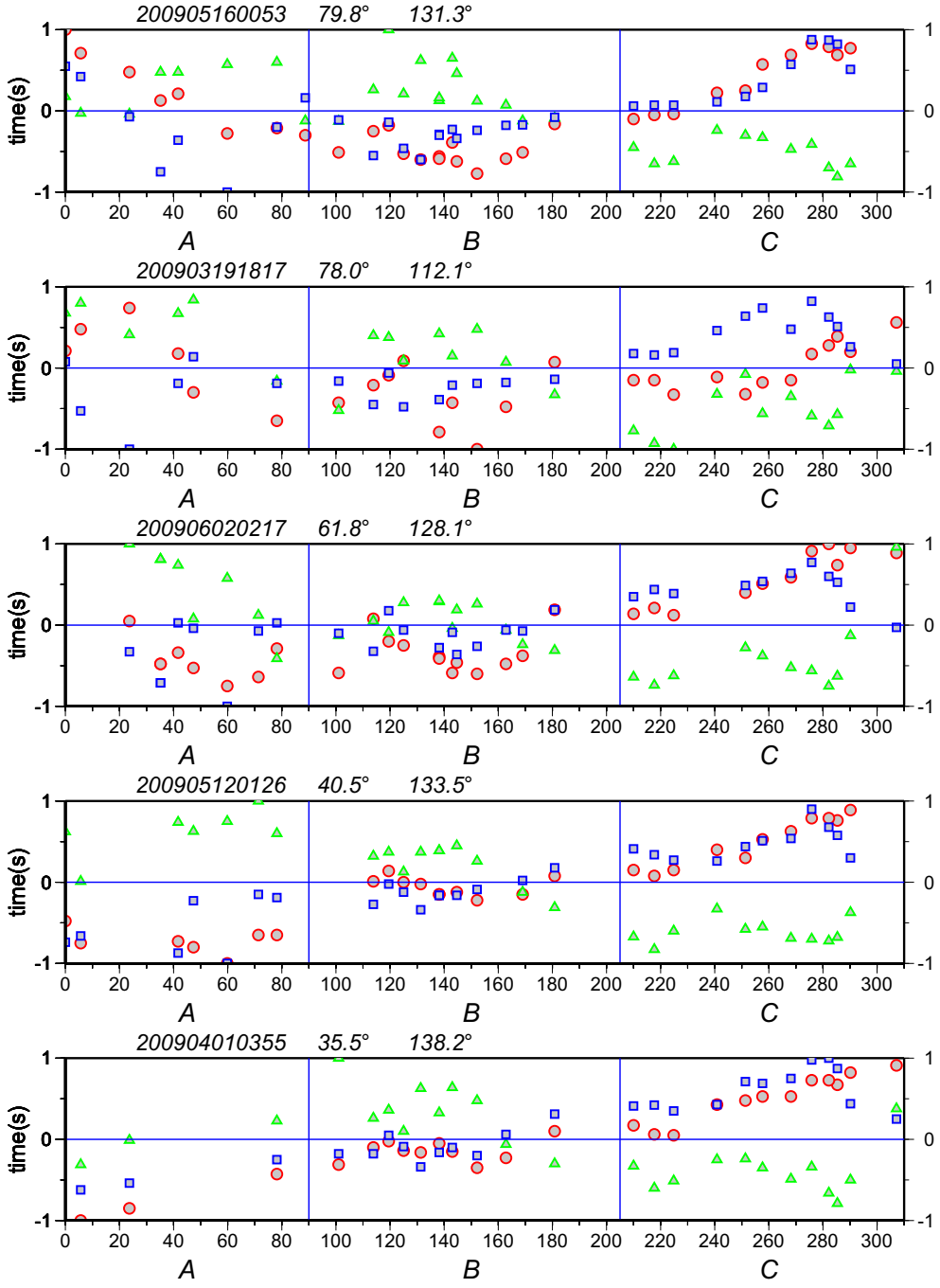

Fig. 6. Patterns of relative arrival time (red circles, scale to left), amplitude (blue squares, scale to right) and pulse width (green triangles, scale to right) for the five SE teleseismic earthquakes, in order of decreasing epicentral distance from top down. All are differential values relative to those of the Sumatra earthquake and are shown as normalized deviation relative to the mean of the same earthquake. Event date, epicentral distance, and back azimuth, respectively, are shown above each panel. The *x*-axis is distance in km, relative to the southernmost station, and the division into A, B, and C groups follows that of Fig. 1. (For interpretation of the references to colour in this figure legend, the reader is referred to the web version of this article.)

compatible with relative ray lengths within slab material as a function of earthquake as derived by ray-tracing. More importantly, for all SE earthquakes, the unknown slab-ray lengths of group B stations consistently exhibit dif_art and dif_amp with greater reduction than those of group C stations and somewhat comparable to those of group A stations. This is evidence of the existence of subducting slab beneath central Taiwan, because both group A stations and group C stations are expected to experience a certain amount of slab-ray lengths. To further quantify this argument, using ray tracing results for group A and C stations (Fig. 2), we conduct a grid search to find the optimal average slab-ray lengths of group B stations that best fit the pattern of observed dif_art (normalized deviation) for each earthquake, assuming velocity of 8 km/s and a 7.5% fast anomaly for slab material. Results show that, for all SE earthquakes, the slab-ray lengths must be at least 150 km for group B stations to fit the dif_art patterns (Fig. 8). The results are applicable for ~80° earthquakes and for ~40° earthquakes, suggesting that fast anomalies beneath central Taiwan are likely to be broad.

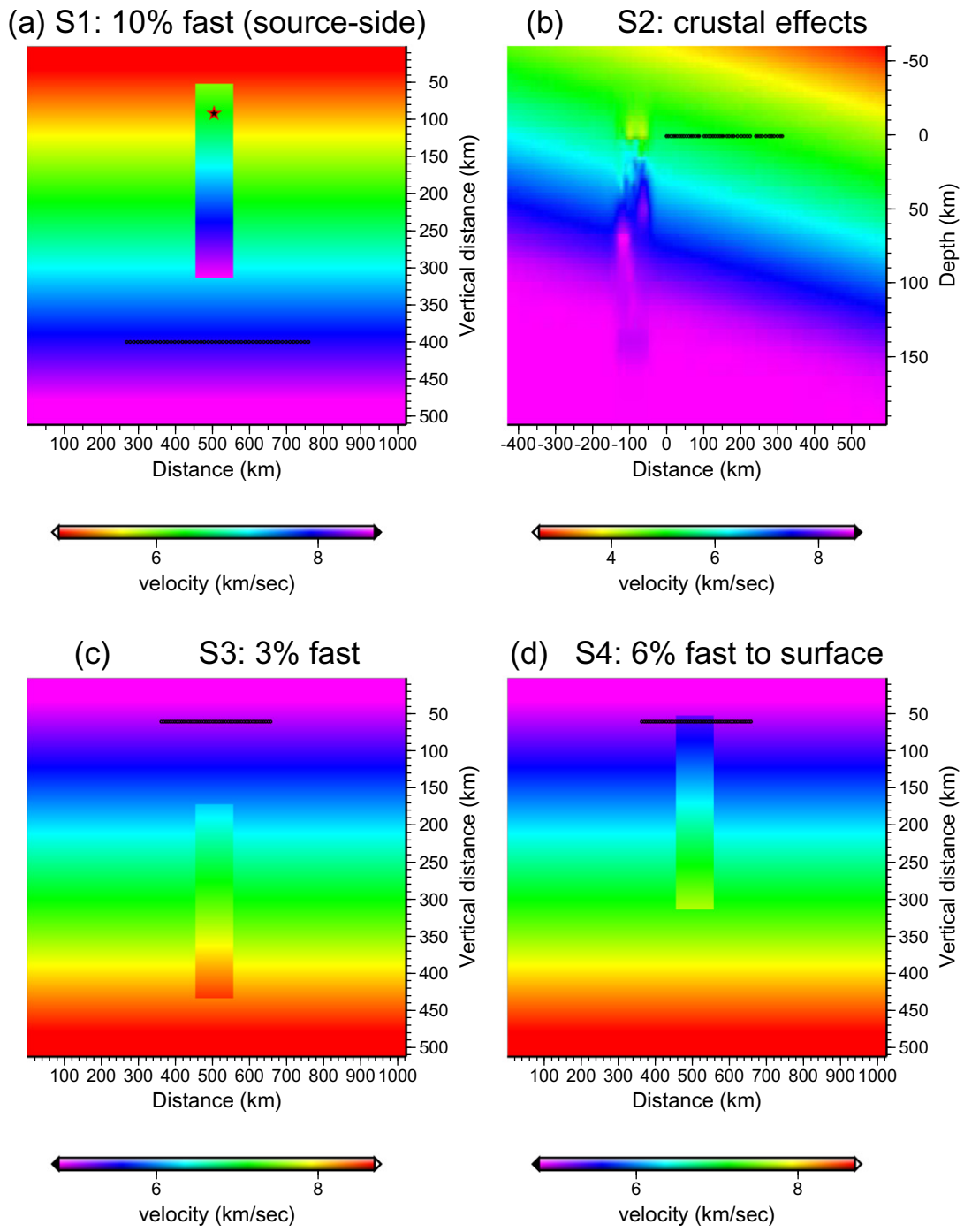

Fig. 7. Velocity models for four scenarios, devised to assess their respective waveform effects. Scenario one (S1) employs a point source located at red star; upwardly propagating plane waves are used for the other three scenarios. Horizontal line of black dots represents virtual array locations. In (c) and (d), the virtual array is placed at 50 km from the top boundary, to avoid boundary effects.

3.3. Waveform effects for crustal heterogeneity, source-side slab, and receiver-side slab

The simulated waveforms as recorded by the virtual array for each scenario are analyzed in the same manner as those of observations. For scenarios 1, 3, and 4, discrepancies relative to those of the 1-D homogeneous case are shown, while for scenario 2, deviations from the means are shown (Fig. 9). The waveform effects of lateral heterogeneities down to 200 km (scenario 2), including crust and uppermost mantle, act primarily on the arrival times and only secondarily on the amplitudes and pulse widths for the ~5 s wave. The waveform effects of slab material (scenarios 1, 3, and 4), at both receiver and source side, all display a point-to-point positive correlation between relative arrival times and amplitudes as well as a negative correlation between amplitudes and pulse widths, which in turn justifies the application of Gaussian fitting. However, the waveform effects of slab material differ in detail at the source side and at the receiver side. While amplitudes and arrival times are always reduced due to effects of source-side slab (scenario 1), consistent with a previous study (Vidale, 1987), the effects of receiver-side slab exhibit only arrival-time reduction while the amplitudes at some particular locations are enhanced

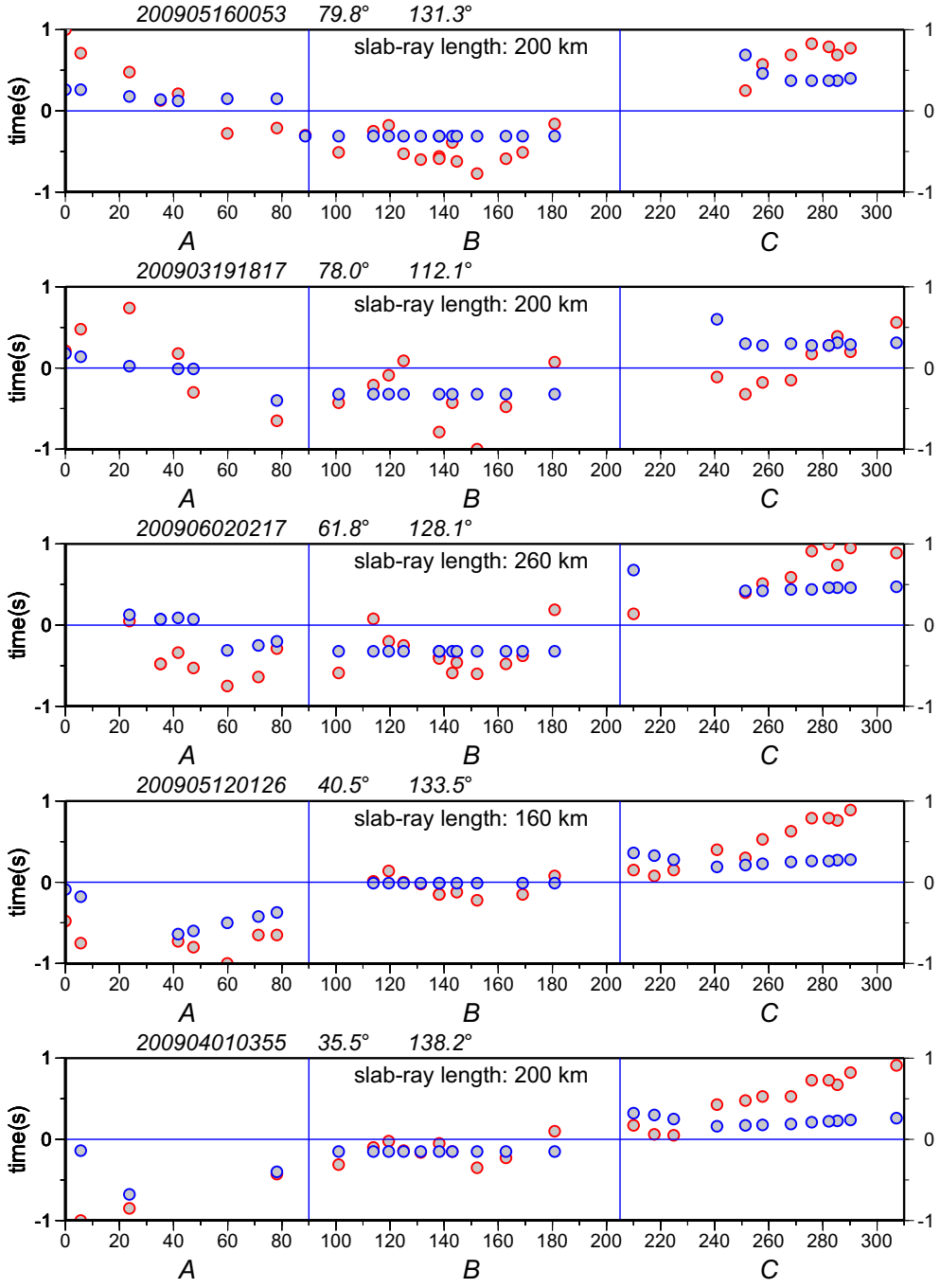

Fig. 8. Comparison of observed patterns of normalized dif_art (red circles) and the best fitting normalized patterns (blue circles) determined by grid-search of average slab-ray lengths for group B stations. The optimal value of slab-ray length is indicated for each event. The *x*-axis is distance in km, relative to the southernmost station.

and coupled with narrowing of pulse widths. This is a conclusion that has not been well documented and is thus worthy of further investigation. We offer an explanation in the discussion below.

4. Discussion

In this study, we use teleseismic first arrivals as recorded by the TAIGER dense linear array to study the waveform effects of receiver-side slab material and to constrain the upper mantle seismic velocity beneath central Taiwan. Ray-tracing results indicate that, given the tectonic setting of Taiwan, slab-induced distortion of teleseismic waveforms is expected from specific azimuths, and this is confirmed by observations (Fig. 3). In order to quantify the waveform information and to avoid potential failure of traditional applications (VanDecar and Crosson, 1990) due to distortion, we employed Gaussian fitting to determine the arrival time and pulse width of first P. Coupling these with a measure of amplitude, the correlation or non-correlation of variation patterns of the three parameters can be used to distinguish between slab effects and crustal effects (Fig. 9). Having eliminated the crustal effects using differential observations, the correlated variation patterns suggest that slabs are the primary heterogeneous structures in the upper mantle in the vicinity of Taiwan. Both qualitative arguments and quantitative assessments require the presence of slab material in

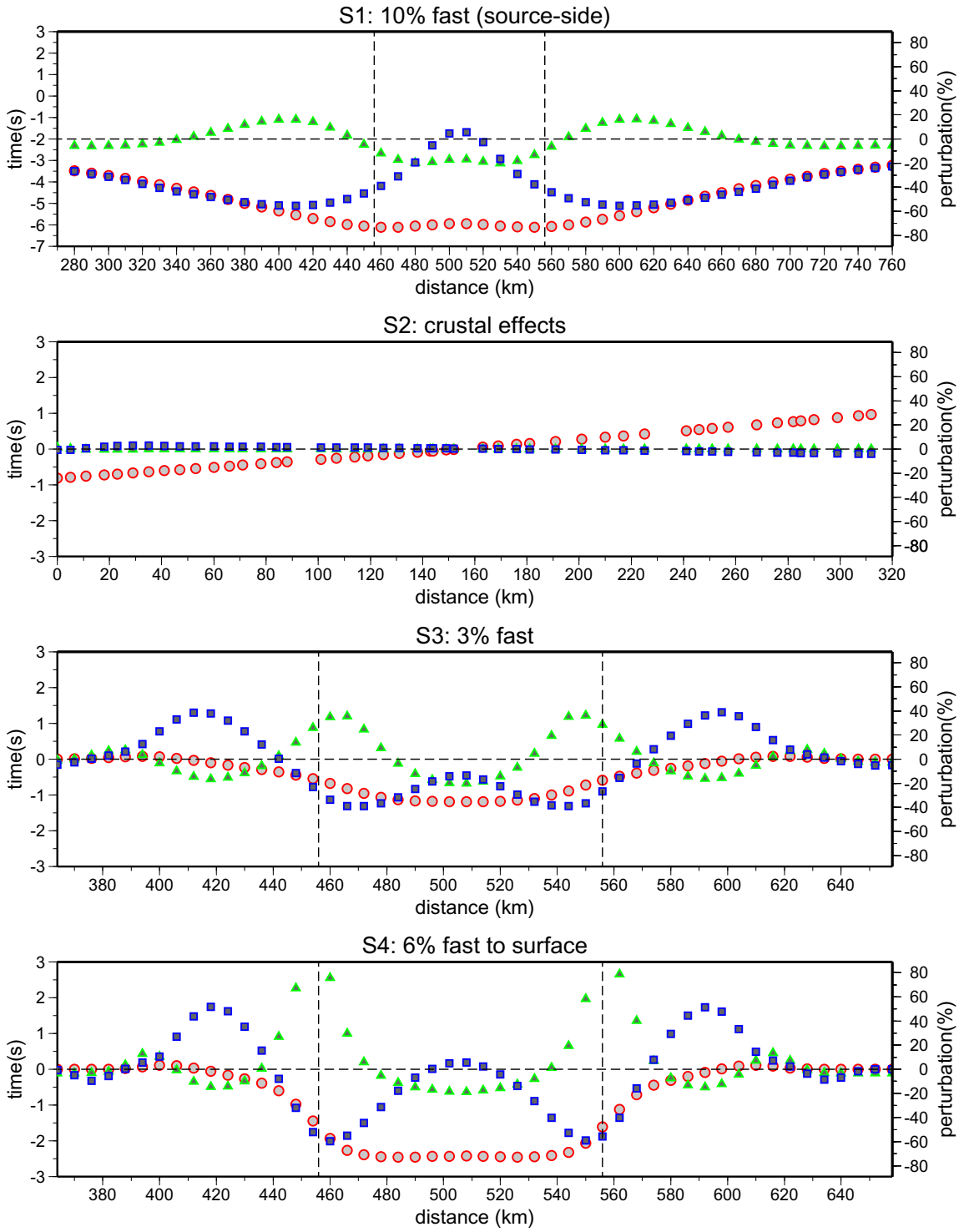

Fig. 9. Perturbed arrival time (red circles, left scale), pulse width (green triangles, right scale), and amplitude (blue squares, right scale) for the four scenarios in Fig. 7. The two vertical dashed lines for scenarios 1, 3, and 4 indicate locations of projected slab boundaries. (For interpretation of the references to colour in this figure legend, the reader is referred to the web version of this article.)

the upper mantle beneath central Taiwan, in order to produce significant effects as observed in group B stations. This is consistent with results of previous studies (Chen et al., 2004, 2011; Wang et al., 2009; Kuo-Chen 2011), but ours is the first study to use full waveform information to address the question. The conclusion itself favors the thin-skinned model for Taiwanese orogeny, as outlined in the introduction and further illustrated here in Fig. 10. Although a more quantified structure is not yet available, this may be accomplished in the near future using waveform inversion by providing independent constraints from data that are sensitive to velocity contrasts. Finally, it is important to note that, as we draw conclusions by comparison of relative values (normalized deviation from the mean), our assumption of a 100-km slab width is simply for convenience of analysis and need not correspond to the actual slab width.

The realization of Taiwan as a natural laboratory for studying waveform effects of receiver-side slab material and the experiment of using TAIGER data for this purpose constitute an unanticipated

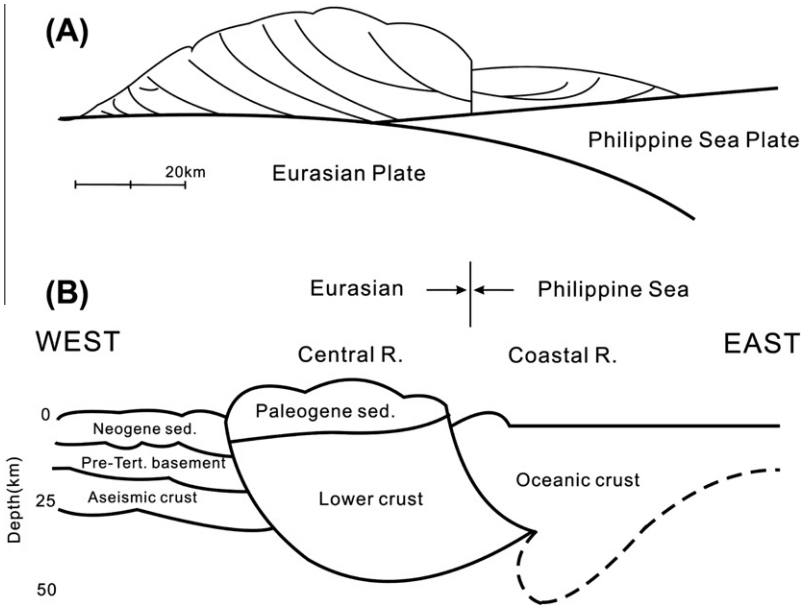

Fig. 10. (a) Tectonic cross-section of central Taiwan, after Fig. 10 of Davis et al. (1983). In this thin-skinned model, orogeny is due to deformation of the accretionary wedge, in a setting typical of passively subducting lithosphere. (b) Schematic cross-section of lithospheric collision model, after Fig. 16 of Wu et al. (1997). In this thick-skinned model, lithospheres of both the Philippine Sea and Eurasian plates are engaged in collision, without subduction of either plate.

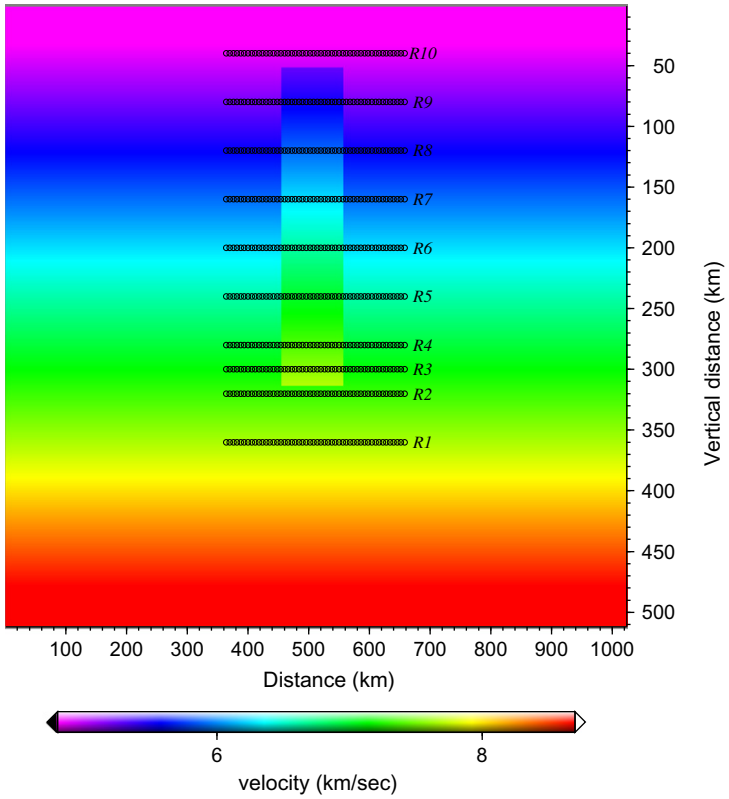

Fig. 11. The series of virtual arrays (*R1* to *R10*) deployed for scenario 4, to continuously monitor the progressive waveform effects of slab upon an upwardly propagating plane wave.

but important by-product of the TAIGER project, which may contribute significantly to our understanding of seismic wave propagation. As mentioned in the Section 1, although the waveform effects of slab material are well established numerically (Vidale, 1987) and such observations have been employed to investigate the deepest extent of down-going slabs in order to address the style of mantle convection (Silver and Chan, 1986; Lay and Young, 1989; Weber, 1990), these prior approaches implicitly deal with source-side slab. Somewhat counter-intuitively, as demonstrated by results of simulation, the waveform effects of slab at the receiver side do exhibit minor differences from those at the source side – not simply amplitude reduction for all locations – despite the

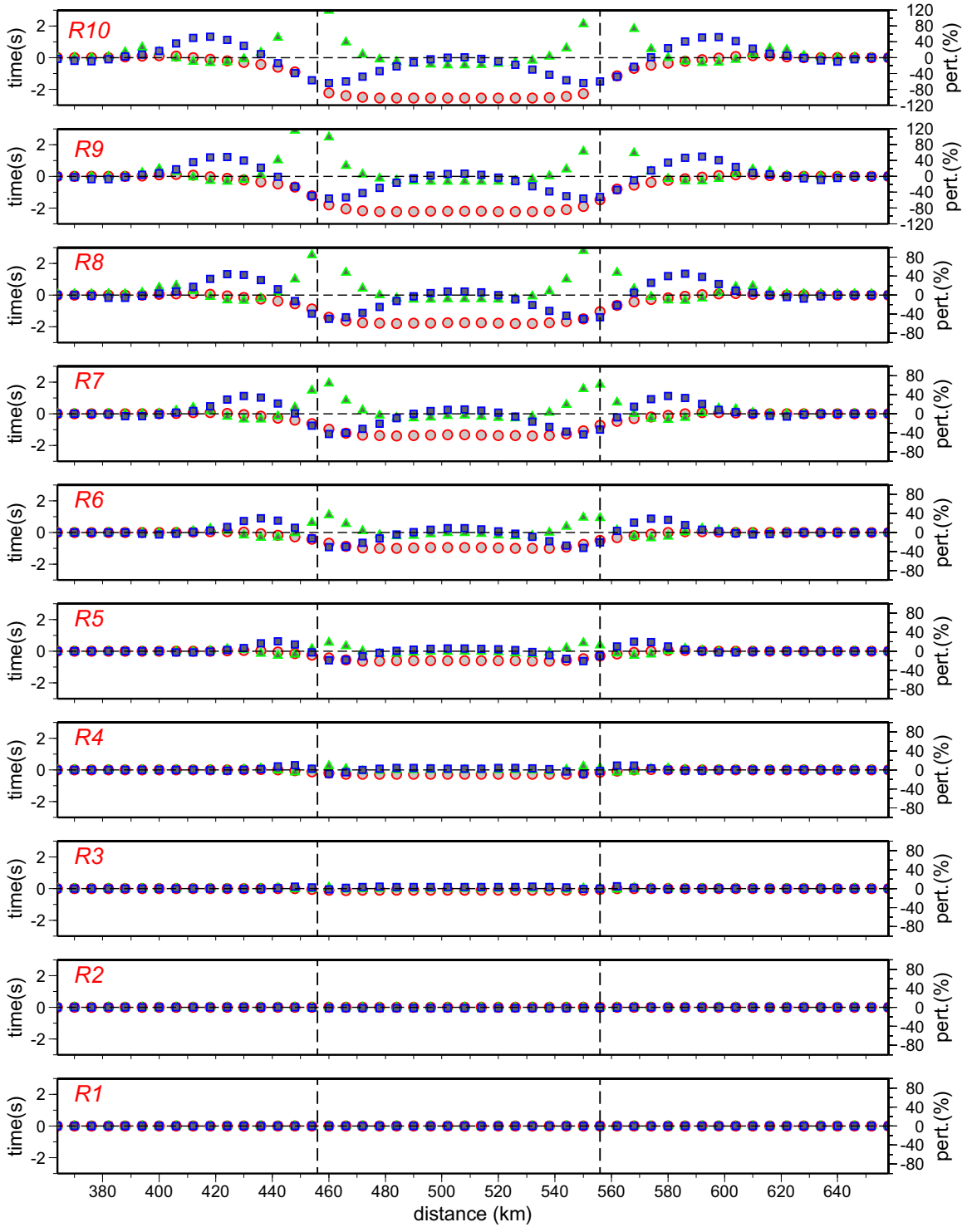

Fig. 12. The resulting perturbations of arrival time, amplitude, and pulse width as shown by the virtual arrays in Fig. 11. Analysis procedures are the same as those for observations, and use of symbols follows that of Fig. 9. Note that locations of amplitude amplification move away from slab boundaries (vertical dashed lines) as the plane wave continues propagating upward with increasing slab effects.

applicability of the same fundamental physics. To explain the amplitude amplification effects of receiver-side slab at some locations, we set up a series of virtual arrays (R1–R10, Fig. 11) to monitor progressive variations of arrival times, amplitudes, and pulse widths for upward propagating plane waves. Having analyzed recorded waveforms in the same manner, we found that the locations of amplitude amplification move away from the slab boundary as the plane wave continues propagating upward with increasing slab effects (Fig. 12). Based on this finding, we propose that the plane wave splits into a fast phase inside the slab and a slow phase outside upon first encountering the slab's bottom boundary. The fast phase continues moving inside the slab while continuously diffracting seismic energy outside the slab. The amplitude amplification is thus caused by constructive interference of the diffracted energy and the later-arriving slow phase. Since the time lags between fast and slow phase increase with slab

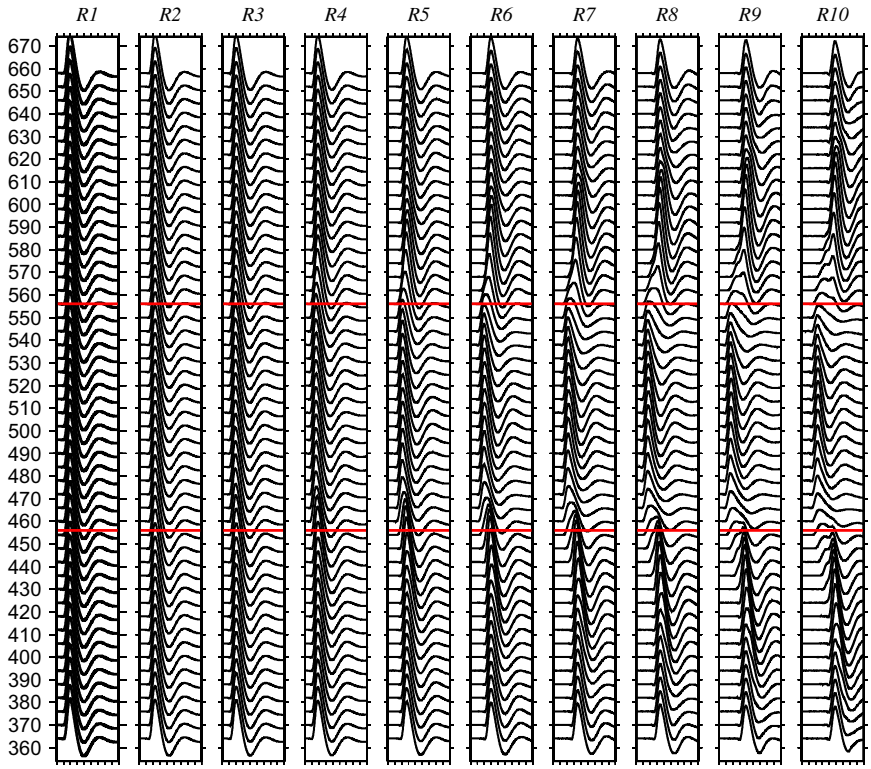

Fig. 13. The waveforms of the upward-propagating plane wave as recorded by the virtual arrays. Vertical axis is distance in km referred to Fig. 11. Note the complexity of waveforms (double peaks) for stations near the slab boundaries (red lines) at *R9* and *R10* arrays. (For interpretation of the references to colour in this figure legend, the reader is referred to the web version of this article.)

effects, the locations of constructive interference move away from the slab boundary through upward propagation. Such mechanisms can also explain the reduced amplitudes and broadening pulse widths at slab side boundaries (Fig. 12). The amplitudes are reduced because both fast and slow phases diffract seismic energy to the other side of the medium, and the pulse widths are broadened because of the differing arrivals of fast and slow phases. [This effect in acoustics is perhaps partly analogous to the "Becke line" effect in optics (Faust, 1955).] When the time lags are quite substantial, we can actually reproduce the bimodal distribution of waveforms (Fig. 13) as observed at stations with distances ranging from 70 to 140 km. Therefore, the observed pulse complexities indeed appear to represent substantial separation, by slab effects, of arrivals of fast and slow phases. This explanation is further supported in that stations between 70 and 140 km tend to exhibit significant reductions in arrival times and amplitudes (Fig. 6). Thus, the results of Gaussian fitting as affected by waveform complexities yield true reflections of slab effects, and the applicability of Gaussian fitting is not compromised by the waveform complexities. Proposed future extensions of this study include using data from other TAIGER arrays and incorporating observations of S waves.

5. Conclusions

The recognition of Taiwan as a natural laboratory for studying receiver-side slab waveform effects has been elaborated by results from tracing rays interacting with slab contours. These also distinguish variation patterns between EUP slab and PSP slab for SE earthquakes – greater effects of EUP slab for the ∼40° earthquakes than for the ∼80° earthquakes, while the effects of PSP slab are about the same for both ∼40° and ∼80° earthquakes where their incident rays approach the dip direction. We apply Gaussian fitting of first P to measure arrival times and pulse widths. When examined for SE earthquakes, using the western earthquake as a reference to eliminate crustal effects, the correlated variation of arrival time and amplitude and their anti-correlation with pulse width indicate that slab effects are dominant. The variation patterns as a function of earthquake not only confirm previous elaborations but also suggest the presence of slab in the upper mantle beneath central Taiwan, as both argued qualitatively and assessed quantitatively. Upon simulation of 2-D wave propagation, we conclude that the lateral heterogeneity of crust and uppermost mantle primarily contribute to variations in arrival time and only secondarily to changes in amplitude and pulse width. Both amplitudes and arrival times are always reduced due to effects of source-side slab material, but the effects of receiver-side slab demonstrate consistent arrival-time reduction while the amplitudes at some particular locations are enhanced and coupled with pulse-width narrowing. Finally, the observed waveform complexity (multiple peaks) can be explained by stations near the slab boundary experiencing significant slab effects.

Acknowledgement

We acknowledge the reviewers and the Editor for their suggestions that significantly improve the manuscript. This work was supported by the Taiwan Earthquake Research Center (TEC) funded through National Science Council (NSC) with grant number 99-2116-M-008-040. The TEC contribution number for this article is 00080. Many of the figures herein was produced using the GMT software of Wessel and Smith (1998).

References

Bijwaard, H., Spakman, W., Engdahl, E.R., 1998. Closing the gap between regional and global travel time tomography. J. Geophys. Res. 103, 30,005–30,078.

Chen, P.-F., Huang, B.-S., Liang, W.-T., 2004. Evidence of a slab of subducted lithosphere beneath central Taiwan from seismic waveforms and travel times. Earth Planet. Sci. Lett. 229, 61–71.

Chen, P.-F., Huang, B.-S., Chaio, L.-Y., 2011. Upper mantle seismic velocity anomaly beneath southern Taiwan as revealed teleseismic relative arrival times. Tectonophysics 498, 27–34.

Davis, D., Suppe, J., Dahlen, F.A., 1983. Mechanics of fold-and-thrust belts and accretionary wedges. J. Geophys. Res. 88, 1153–1172.

Ekström, G., Dziewonski, A.M., Maternovkaya, N.N., Nettles, M., 2005. Global seismicity of 2003: centroid-moment-tensor solutions for 1087 earthquakes. Phys. Earth Planet. Inter. 148 (1–2), 327–351.

Faust, R.C., 1955. Refractive index determinations by the central illumination (Becke line) method. Proc. Phys. Soc. B 68, 1081–1094.

Ho, C.S., 1986. A synthesis of the geologic evolution of Taiwan. Tectonophysics 125, 1–16.

Huang, B.-S., 1992. A program for two-dimensional seismic wave propagation by the pseudospectrum method. Comput. Geosci. 18, 289–307.

Hung, S.-H., Dahlen, F.A., Nolet, G., 2001. Wavefront healing: a banana-doughnut perspective. Geophys. J. Int. 146, 289–312.

Lay, T., Young, C.J., 1989. Waveform complexity in teleseismic broadband SH displacements: slab diffractions or deep mantle reflections? Geophys. Res. Lett. 16, 605–608.

Kennett, B.L.N., Engdahl, E.R., Buland, R., 1995. Constraints on seismic velocities in the Earth from travel times. Geophys. J. Int. 122, 108–124.

Kuo-Chen, H., 2011. Imaging Deep Structures Under the Taiwan Orogen: Toward Tectonic Model Testing. Ph.D. thesis. Binghamton University, State University of New York, p. 175.

Lallemand, S., Font, Y., Bijwarrd, H., Kao, H., 2001. New insights on 3-D plates interaction near Taiwan from tomography and tectonic implications. Tectonophysics 335, 229–253.

Li, C., van der Hilst, R.D., 2010. Structure of the upper mantle and transition zone beneath Southeast Asia from traveltime tomography. J. Geophys. Res. 115, B07308. doi:10.1029/2009JB006882.

Lin, C.-H., 2009. Compelling evidence of an aseismic slab beneath central Taiwan from a dense linear seismic array. Tectonophysics 466, 205–212.

Malavieille, J., Lallemand, S., Domingues, S., Deschamps, A., Lu, C.-Y., Liu, C.-S., Schnurle, P., Crew, A.S., 2002. Arc-continent collision in Taiwan: new marine observations and tectonic evolution. Geol. Soc. Am Spec. Pap. 358, 189–213.

Okaya, D., Wu, F., Wang, C.-Y., Yen, H.-Y., Huang, B.-S., Brown, L., Liang, Liang.W.-T., 2009. Joint passive/controlled source seismic experiment across Taiwan. Eos Trans. AGU 90 (34). doi:10.1029/2009EO340001.

Rawlinson, N., de Kool, M., Sambridge, M., 2006. Seismic wavefront tracking in 3D heterogeneous media: applications with multiple data classes. Explor. Geophys. 37, 322–330.

Sigloch, K., Nolet, G., 2006. Measuring finite-frequency body-wave amplitudes and traveltimes. Geophys. J. Int. 167, 271–287.

Silver, P.G., Chan, W.W., 1986. Observations of body wave multipathing from broadband seismograms: evidence for lower mantle slab penetration beneath the sea of Okhotsk. J. Geophys. Res. 91 (B14), 13,787–13,802.

Song, T.-R.A., Helmberger, D.V., 2007. Validating tomographic model with broadband waveform modeling: an example from the LA RISTRA transect in the southwestern United States. Geophys. J. Int.. doi:10.1111/j.1365-246X.2007.03508.x.

Suppe, J., 1981. Mechanics of mountmain building and metamorphism in Taiwan. Geol. Soc. China 4, 67–89.

Teng, L.S., 1990. Geotectonic evolution of Late Cenozoic arc-continent collision in Taiwan. Tectonophysics 183, 57–76.

VanDecar, J.C., Crosson, R.S., 1990. Determination of teleseismic relative arrival times using multi-channel cross-correlation and least squares. Bull. Seismol. Soc. Am. 80, 150–169.

Vidale, J.E., 1987. Waveform effects of a high-velocity, subducted slab. Geophys. Res. Lett. 14, 542–545.

Wang, Z., Fukao, Y., Zhao, D., Kodaira, S., Mishra, O.P., Yamada, A., 2009. Structural heterogeneities in the crust and upper mantle beneath Taiwan. Tectonophysics 476, 460–477. doi:10.1016/j.tecto.2009.07.018.

Weber, M., 1990. Subduction zones – Their influence on traveltimes and amplitudes of *P*-waves. Geophys. J. Int. 101, 529–544.

Wessel, P., Smith, W.H.F., 1998. New, improved version of generic mapping tools released. Eos Trans. Am. Geophys. U. 79 (47), 579.

Wu, F.T., Rao, R.J., Salzberg, D., 1997. Taiwan orgeny: thin-skinned or lithospheric collision? Tectonophysics 274, 191–220.

Wu, Y.-M., Chang, C.-H., Zhao, L., Shyu, J.H., Chen, Y.-G., Sieh, K., Avouac, J.-P., 2007. Seismic tomography of Taiwan: improved constraints from a dense network of strong motion stations. J. Geophys. Res. 112, B08312. doi:10.1029/2007JB004983.